Tsunami and tephra deposits record interactions between past eruptive activity and landslides at Stromboli Volcano

Marco Pistolesi[1], Antonella Bertagnini[2], Alessio Di Roberto[2], Maurizio Ripepe[3] and Mauro Rosi[1]

[1]Dipartimento di Scienze della Terra, Università di Pisa - 56126 Pisa (Italy)

[2]Istituto Nazionale di Geofisica e Vulcanologia - 56125 Pisa (Italy)

[3]Dipartimento di Scienze della Terra, Università di Firenze - 50121 Firenze (Italy)

ABSTRACT

Devastation associated with tsunamis is well known on the global scale. Flank collapse at volcanic islands is among the mechanisms triggering tsunamis but very few examples document interaction between landslides and volcanic activity. The study of three well-preserved medieval tsunami deposits recently discovered along the coast of Stromboli Volcano (Aeolian Islands, southern Italy) enabled a detailed characterization of the tsunami sequences intercalated with volcaniclastic deposits and primary tephra and reconstruction of the likely sequence of volcanic events. In one case a violent explosion possibly preceded the tsunami, whereas in the youngest event, the lateral collapse of the volcano flank triggered a tsunami wave that was rapidly followed by sustained explosive magmatic activity and ensuing prolonged ash venting. The hypothesized tsunami-triggering dynamics suggests a close link between volcanic activity and flank collapse, further confirming that the persistent activity at Stromboli makes the volcano particularly susceptible to tsunami generation.

INTRODUCTION

Before the seminal works by Atwater (1987) and Dawson et al. (1988), studies on tsunami deposits were mostly isolated post-disaster reports. Widely occurring layers of sand and gravel were typically interpreted as marine transgression events or as storm surges of extraordinary magnitude. Tsunami deposits are the main evidence of past tsunami wave inundations but are inherently difficult to identify in coastal sediment sequences (Bardet et al., 2003; Dawson and Stewart, 2007; Shiki et al., 2008; Matsumoto et al., 2016). Landslides occurring on steeply sloped coastal areas, including coastal volcanoes or volcanic islands, have been shown to produce devastating tsunamis (Hoshizumi et al., 1999; Satake and Kato, 2001,Ward and Day, 2003; Paris et al., 2014; Day et al., 2015; Walter et al., 2019). Surprisingly, there are only a few clear examples worldwide of the relationship between volcanic activity and landslide generation (Paris et al., 2017).

We focus here on the volcanic island of Stromboli (Southern Tyrrhenian Sea) where at least six small-scale tsunamis have occurred since 1900 (Maramai et al., 2005). The largest tsunami of the last century was initiated on 30 December 2002 by two landslides that detached from the submarine and subaerial flanks of the Sciara del Fuoco (SdF) scar (Tinti et al., 2006; Marani et al., 2008). Stromboli has been the source of potentially tsunamigenic large-scale flank failures, as revealed by marine (Di Roberto et al., 2010) and subaerial records (Tibaldi, 2001). Rosi et al. (2019) recently identified three well-preserved medieval tsunami deposits on the NE coast of the island. We present here a complete sedimentological characterization of these tsunami deposits, coupled with a detailed investigation of the intercalated primary volcanic layers. These extremely well preserved tsunami beds document the close link between volcanic events and

tsunamigenic landslides and, in general, indicate that volcanic activity can destabilize volcanic slopes. Results may help better design research on other active volcanic islands and mitigation strategies.

METHODS

Field analyses were conducted in three 2m-deep trenches with a cumulative extension of 80 m, dug in a broadly flat area located on the back side of a coastal dune 1-2 m above sea level (a.s.l.; Figs. 1, DR1). The maximum clast size was determined by measuring the three axes of pebbles collected from selected layers at six sites in the trenches. Nineteen samples were recovered and mechanically dry-sieved for grain-size analyses (Fig. DR2, Table DR1); components and clast shape parameters were determined under a stereomicroscope and by two-dimensional image analysis. Matrix glass compositions of scoriaceous lapilli were determined using an energy-dispersive micro-analytical system (Data Repository).

TSUNAMI DEPOSIT CHARACTERISTICS

The trenches crossed a laterally continuous succession of unconsolidated sediments consisting of massive, fine-grained volcaniclastic deposits intercalated with primary ash and lapilli (Fig. DR1). Three black-sand sheet deposits containing scattered rounded pebbles occur within the succession. These were interpreted as tsunamiites on the basis of the sedimentary structures that commonly characterize such deposits (e.g., erosional basal contacts, landward dispersal, texture and grading, stratification, boulder accumulation, sediment composition; Dawson and Shi, 2000; Morton et al. 2007; Peters and Jaffe, 2010; Engel and Bruckner, 2011). Their sharp contact with the continental fine-grained ash also excludes any links to erratic shoreline migrations (marine

69 transgression-regression cycles). Although the distinction between tempestites and tsunamiites is
70 not always straightforward, the limited 50 km-wide marine fetch which separates Stromboli from
71 the eastern and southern coasts of Italy makes them unlikely storm deposits.
72 On the basis of ^{14}C data obtained from charcoal below the tsunami beds, along with historical
73 accounts and geological and archaeological evidence, Rosi et al. (2019) suggested these tsunamis
74 occurred between the 14th and 15th century.
75 The Lower Tsunami deposit (LTd) is the thickest, coarsest and laterally most continuous bed,
76 covering a longitudinal distance to the coastline of 60 m. The deposit locally shows an erosive
77 base (Fig. DR1) and bears cm-size fragments of pottery and sporadic angular lava fragments.
78 The maximum thickness is ~30 cm in Trench 2 and gradually decreases to <5 cm in the higher
79 sites of Trench 1 (230 m from coastline; 2.8 m a.s.l.; Fig. 2). In Trench 3, the LTd comprises two
80 normally-graded, medium to coarse sand beds, one 4 cm thick and the other 13 cm thick,
81 overlain by a 17 cm-thick reversely-graded bed of coarse sand with scattered rounded lava
82 pebbles that can be traced continuously inland to Trench 1, where it is 0-15 cm thick.
83 The Intermediate Tsunami deposit (ITd) occurs only in Trench 3 (Fig. 1). It consists of a 4 cm-
84 thick, coarse, black sand with sporadic cm-sized rounded pebbles.
85 The Upper Tsunami deposit (UTd) comprises a normally graded, poorly sorted, medium to
86 coarse sand with an erosive base and containing variable amounts of pebbles and cobbles (Fig.
87 DR1) and a higher abundance of angular juvenile clasts than LTd and ITd. It can be traced up to
88 220 m inland (3.5 m a.s.l.) of the present shoreline.
89 LTd and UTd thickness rapidly decreases inland. In LTd, this is coupled with an increase in
90 deposit sorting and a decrease in the average matrix grain-size, with grain-size distribution
91 identical to that of the present-day beach sand (Figs. 2, 3A). The maximum clast size in the

tsunami deposits decreases progressively landward (Figs. 2, 3B). LTd contains the largest clasts, ITd and Utd the smallest and least variable clasts (Fig. 3C). Morphological parameters indicate that most of the clasts are spherical to partially oblate, irrespective of distance from the shoreline (Fig. DR3), much like the coarsest fraction of the present beach deposit. A linear relationship exists among form factor and convexity (Fig. DR3), with the UTd clasts having the largest morphological variability; this agrees with the occurrence of more irregularly-shaped scoria fragments in UTd, and with the greater abundance of smooth, rounded lava clasts in LTd and ITd (Fig. DR4).

The components of the sand fraction in the three tsunami deposits are similar and comprise slightly rounded and abraded dense, black glass (40 wt.%), crystals of clinopyroxene (30 wt.%), olivine (20 wt.%) and minor plagioclase, as well as rare red, oxidized lava fragments. The components and their relative abundances, including the lack of macro- and micro-bioclasts, are remarkably similar to those of sand forming the present beach (Fig. DR5).

VOLCANIC AND LANDSLIDE ACTIVITY AT STROMBOLI

Two primary lapilli-bearing tephra fallout sequences, T1 and T2, were found below LTd and above UTd, respectively (Fig. 1). T1 consists of cm-sized, banded light- and dark-colored pumice lapilli (T1pm) overlain by a discontinuous, <2 cm reddish ash (T1a) bed consisting of fresh-to-altered lava, scoria, holocrystalline rock fragments and loose crystals. Most T1a scoria fragments show a µm-thick rim of leached glass characterized by Al_2O_3 loss and SiO_2 gain: an indication of acidic alteration by magmatic gases from the crater area (Wyering et al., 2014; Fig. 4A-D). T1 rests on a soil and is in places separated from LTd by a 2-3 cm-thick, fine-grained muddy sediment containing small charcoals, suggesting either a time lapse between the

explosive eruption and the tsunami or syn-eruptive mud deposition. T2 consists of a plane-parallel bedset composed of three distinct fallout layers (T2a, 2b and 2c from base to top). T2a is a 4 cm-thick, fine to medium ochre-colored ash lying directly above UTd; sparse pumice fragments occur at the top of the layer (T2pm). T2 was also found higher on the volcano slopes, where T2a bears pumice and scoriaceous bombs. T2a particles >500 μm consist of fresh, vesicular scoriae typical of summit explosive activity. The fraction <500 μm consists of fresh to weakly altered lava and scoria fragments, possibly resulting from the breakage and comminution of volcanic rocks that did not undergo summit alteration. T2b is a 2-3 cm-thick, well-sorted layer of coarse ash to fine lapilli mainly composed of fresh, variably vesicular black scoriae. T2c is a 5-6 cm-thick, vesiculated, fine reddish-brown ash composed of fresh to hydrothermally-altered lavas and scoriae, loose crystals and holocrystalline volcanic rock fragments.

The matrix glass composition of fresh scoriaceous lapilli (Fig. 4E) shows the typical variability of the high-porphyritic (HP) magma feeding persistent activity at Stromboli (Métrich et al., 2010). Mingled pumices (T1pm and T2pm) contain HP material mingled with the less evolved composition of the low-porphyritic (LP) magma emitted only during Strombolian paroxysms (Métrich et al., 2010).

Sequences T1 and T2 are interpreted as deriving from transient high-energy Strombolian paroxysms that emplaced mingled pumices (T1pm, T2pm), followed by a fallout of red ash (T1a, T2c), as observed during the 1930, 2003 and 2007 eruptions (Rittman, 1931; Rosi et al., 2006; Pistolesi et al., 2011) and in the deposits of older paroxysms. Within T2a, the coexistence of fresh, vesicular scoriae typical of activity at the summit and of fresh to weakly altered lava and scoria fragments suggests that it formed through the simultaneous fall of juvenile material from an eruptive column and dust-rich ash clouds related to subaerial landslides, as observed in a

similar deposit from the December 2002 activity analyzed for comparison. While LTd was possibly immediately preceded by a paroxysmal event (T1), the T2 eruptive succession represents a tsunami-triggering landslide that emplaced UTd and T2a, immediately followed by a paroxysmal event (T2pm, T2b, T2c). The synchronous occurrence of the landslide and paroxysmal activity is further corroborated by the coeval sedimentation of ash from the landslide and scoriaceous and pumice fragments that coarsen uphill, as observed in several outcrops.

DISCUSSION

Field evidence indicates that the tsunami waves deeply eroded the beach and dune deposits as they penetrated inland. The progressive loss of carrying capacity led to deposition, as also demonstrated by the systematic decrease in the maximum diameter of clasts and deposit thickness. Considering the proximity of the sites to the likely source area, and given that tsunami generation from landslides possibly involves more than one wave of notable amplitude and erosion capacity, single normal gradation (UTd) or repeated inversely-graded units (LTd) may be ascribed either to a complex tsunami wave from a single landslide event or to a multi-stage landslide failure mechanism.

Large landslides have repeatedly occurred at Stromboli in the past, as demonstrated by onshore geological evidence (Tibaldi, 2001) and marine sediment records (Di Roberto et al., 2010), suggesting that the studied tsunamis were possibly caused by large-scale landslides in the NW sector of the volcano. Among the landslides in the last 5 ka that generated turbidity currents in distal sites (Di Roberto et al., 2010), two major events stand out. The older event is attributed to the collapse of Neostromboli (~5 ka), whereas the younger one occurred ~1 ka ago, both in agreement with geological subaerial evidence (Arrighi et al., 2004; Speranza et al., 2008).

Interestingly, the ~1 ka turbidite is comparable in age to the medieval tsunamis studied here. The turbidite found in marine cores 24 km from SdF may have resulted from the stacking of three distinct turbidites cogenetic with volcanic landslides at Stromboli, which produced LTd, ITd and UTd. This agrees with the structure of the turbidite, showing at least three stacked, closely spaced sandy units with a sharp base and gradational top (Di Roberto et al., 2010). Although large-volume turbidites resulting from landslides may incorporate variable amounts of sediment due to seafloor and slope erosion, thereby increasing their final volume (Hunt et al., 2011), the small volume of the Stromboli landslides coupled with the proximity of the coring site suggest a first-order correlation between turbidite thickness and landslide volume, as in the known 2002 event (2-3 cm for ~30 Mm^3). We estimate a total volume of ~180 Mm^3 for the three medieval events: this should be considered a conservative estimate due to the potential erosive activity of the turbidity currents and deposit compaction.

Although we cannot exclude seismic triggers for past slope destabilization, recent eruptive crises at Stromboli suggest that deformation of the volcano flanks linked to magmatic injection is the most probable cause of flank instability. During the 2002-03, 2007 and 2014 eruptions, the injection of magma eventually determined the seaward displacement of a small sector of the SdF and the opening of lateral effusive vents (Calvari et al., 2008; Ripepe et al. 2015; Valade et al., 2017). The significant inflation of the volcano flank culminated on 30 December 2002 with a tsunamigenic landslide. The occurrence of three large-scale tsunamigenic landslides in one century suggests that a high magma discharge rate in that period led to the deposition of a large amount of loose material in a narrow sector of the volcano. The close correlation between the two violent explosions and the tsunamis further suggest a higher magma supply rate. Although the T1-LTd sequence does not provide conclusive evidence, it suggests that a high supply rate

resulted in a paroxysmal explosion followed by flank deformation and a tsunamigenic landslide. The UTd-T2 sequence better indicates that possible flank deformation may result in a tsunamigenic landslide rapidly followed by violent explosive activity. Flank collapses have been successfully linked to subsequent explosive eruptions at Tenerife (Paris et al., 2017) and more recently at Anak Krakatau (Walter et al., 2019). In the case of the 170 ka Tenerife event, the close relationship between volcanic activity and tsunamigenic landslides was revealed by the occurrence of pumice fragments from the El Abrigo eruption in the topmost part of the turbidity sequence. There are only a few examples of coupled slope instability and explosive activity at volcanic islands, possibly due to the complexity of the deposit sequences and their low preservation potential. The clear, well-preserved succession discovered at Stromboli is an excellent example of such multiple events, during which violent explosions immediately precede or rapidly follow tsunamigenic landslides.

ACKNOWLEDGMENTS

Research was conducted in the framework of the agreements between the Italian Department of Civil Protection with the Unversity of Florence (DEVNET) and INGV (B2, Sub-Task A). We thank A. Di Renzoni and S. Levi for discussions and topographic data. B. Voight, A. Freundt, S. Takarada, I. Manzella and Michael Ort helped improve an early version of the manuscript. We also thank J. Hunt for his encouraging and constructive review.

REFERENCES CITED

Arrighi, S., Rosi, M., Tanguy, J. C. and Courtillot, V., 2004, Recent eruptive history of Stromboli (Aeolian Islands, Italy) determined from high-accuracy archeomagnetic dating: Geophysical Research Letters, v. 31, L19603, p. 1-4.

Atwater, B.F., 1987, Evidence for Great Holocene Earthquakes along the Outer Coast of Washington State, Science, v. 236, p. 942–944.

Bardet, J.P., Synolakis, C.E., Davies, H.L., Imamura, F., and Okal, E.A., 2003, Landslide tsunamis: Recent findings and research directions: Pure Applied Geophysics, v. 160, p. 1793–1809.

Calvari, S., Inguaggiato, S., Puglisi, G., Ripepe, M., and Rosi, M., 2008, The Stromboli Volcano: An Integrated Study of the 2002-2003 Eruption: Geophysical Monograph Series, v. 182, 399 p.

Day, S., Llanes, P., Silver, E., Hoffmann, G., Ward, S., and Driscoll, N., 2015, Submarine landslide deposits of the historical lateral collapse of Ritter Island, Papua New Guinea: Marine Petroleum Geology, v. 67, p. 419–438.

Dawson, A.G., Long, D., and Smith, D.E., 1988, The Storegga slides: Evidence from eastern Scotland for a possible tsunami: Marine Geology, v. 82, p. 271–276.

Dawson, A.G., and Shi, S., 2000, Tsunami Deposits: Pure and Applied Geophysics, v. 157, p. 875-897.

Dawson, A.G., Stewart, I., 2007, Tsunami deposits in the geological record: Sedimentary Geology, v. 200, p. 166–183.

Di Roberto A., Rosi, M., Bertagnini, A., Marani, M.P., and Gamberi, F., 2010, Distal Turbidites and Tsunamigenic Landslides of Stromboli Volcano (Aeolian Islands, Italy), i*n* Mosher D.C.

et al., eds., Submarine Mass Movements and Their Consequences: Advances in Natural and Technological Hazards Research, v. 28. Dordrecht, Springer, p. 719-731.

Engel, M., and Brückner, H., 2011, The identification of palaeo-tsunami deposits – a major challenge in coastal sedimentary research: Coastline Reports, v. 17, p. 65-80

Hoshizumi H., Uto K. and Watanabe K., 1999, Geology and Eruptive History of Unzen Volcano, Shimabara Peninsula, Kuyshu, SW Japan: Journal of Volcanology and Geothermal Research, v. 89, p. 81-94.

Hunt J.E, Wynn R.B., Masson D.G., Talling P.J., Teagle D.A.H., 2011, Sedimentological and geochemical evidence for multistage failure of volcanic island landslides: A case study from Icod landslide on north Tenerife, Canary Islands: Geochemistry, Geophysics, Geosystems, v. 12, p. 1-36

Maramai, A., Graziani, L., and Tinti, S., 2005, Tsunamis in the Aeolian Islands (southern Italy): a review: Marine Geology, v. 215, p. 11-21.

Marani, M.P., Gamberi, F., Rosi, M., Bertagnini, A., and Di Roberto, A., 2008, Deep-sea deposits of the Stromboli 30 December 2002 landslide, *in* Calvari, S., Inguaggiato, S., Puglisi, G., Ripepe, M., and Rosi, M. eds., Stromboli Volcano: an integrated study of the 2002–2003 eruption. Washington DC, American Geophysical Union, Geophysical Monograph 182, p. 157–169.

Matsumoto, D., Sawai, Y., Tanigawa, K., Fujiwara, O., Namegaya, Y., Shishikura, M., Kagohara, K., and Kimura, H., 2016, Tsunami deposit associated with the 2011 Tohokuoki tsunami in the Hasunuma site of the Kujukuri coastal plain, Japan: Island Arcs, v. 25, p. 369–385.

Métrich, N., Bertagnini, A., and Di Muro, A., 2010, Conditions of magma storage, degassing and ascent at Stromboli: New Insights into the volcano plumbing system with inferences on the eruptive dynamics: Journal of Petrology, v. 51, p. 603–626.

Morton, R., Gelfenbaum, G., Jaffe, B., 2007, Physical criteria for distinguishing sandy tsunami and storm deposits using modern examples: Sedimentary Geology, v. 200, p. 184-207.

Paris, R., Wassmer, P., Lavigne, F., Belousov, A., Belousova, M., Iskandarsyah, Y., Benbakkar, M., Ontowirjo, B., and Mazzoni, N., 2014, Coupling eruption and tsunami records: the Krakatau 1883 case study, Indonesia. Bulletin of Volcanology, v. 76, p. 814, doi:10.1007/s00445-014-0814-x

Paris, R., Coello Bravo, J.J., Gonzalez, M.E.M., Kelfoun, K., and Nauret, F., 2017, Explosive eruption, flank collapse and megatsunami at Tenerife ca. 170 ka: Nature Communications, v. 8, p. 1–8, doi:10.1038/ncomms15246.

Peters, R., and Jaffe, B.E., 2010, Identification of tsunami deposits in the geologic record; developing criteria using recent tsunami deposits: U.S. Geological Survey Open-File Report 2010-1239, 39 p.

Pistolesi, M., Delle Donne, D., Pioli, L., Rosi, M., and Ripepe, M., 2011, The 15 March 2007 explosive crisis at Stromboli volcano, Italy: Assessing physical parameters through a multidisciplinary approach: Journal of Geophysical Research, v. 116, no. B12

Ripepe, M., Delle Donne, D., Genco, R., Maggio, G., Pistolesi, M., Marchetti, E., Lacanna, G., Ulivieri, G., and Poggi, P., 2015, Volcano seismicity and ground deformation unveil the gravity-driven magma discharge dynamics of a volcanic eruption: Nature Communications, v. 6, p. 1–6, doi: 10.1038/ncomms7998.

Rittmann, A., 1931, Der Ausbruch des Stromboli am 11 Septem- ber 1930, Zeits Vulkanol., v. 14, p. 47–77.

Rosi, M., A. Bertagnini, A. J. L. Harris, L. Pioli, M. Pistolesi, and M. Ripepe, 2006, A case history of paroxysmal explosion at Stromboli: Timing and dynamics of the April 5, 2003 event: Earth Planet. Sci. Lett., v. 243, p. 594–606.

Rosi, M., Levi, S.T., Pistolesi, M., Bertagnini, A., Brunelli, D., Cannavò, V., Di Renzoni, A., Ferranti, F., Renzulli, A., and Yoon, D., 2019, Geoarchaeological Evidence of Middle-Age Tsunamis at Stromboli and Consequences for the Tsunami Hazard in the Southern Tyrrhenian Sea. Scientific Reports, v. 9, 677.

Satake, K, and Kato, Y., 2001, The 1741 Oshima-Oshima Eruption: Extent and Volume of Submarine Debris Avalanche: Geophysical Research Letters, v. 28, p. 427-430.

Shiki, T., Tachibana, T., Fujiwara, O., Goto, K., Nanayama, F., and Yamazaki, T., 2008, Characteristic features of tsunamiites, *in* Shiki, T., Tsuji, Y., Yamazaki, T., and Minoura, K., eds., Tsunamiites-Features and Implications: Amsterdam, Elsevier, p. 319–340.

Slingerland, R., and Voight, B., 1979, Occurrence and predictive models for slide-generated water waves, *in* Rockslides and Avalanches, Elsevier, Amsterdam, v. 2, pp. 317-400.

Speranza, F., Pompilio, M., Caracciolo, F. D. and Sagnotti, L., 2008, Holocene eruptive history of the Stromboli volcano: constraints from paleomagnetic dating, Journal of Geophysical Research, v. 113(B9), B09101.

Tibaldi, A., 2001, Multiple sector collapses at Stromboli volcano, Italy: how they work: Bulletin of Volcanology, v. 63, p. 112–125.

Tinti, S., Pagnoni, G., and Zaniboni, F., 2006, The landslides and tsunamis of the 30th of December 2002 in Stromboli: Analysed through numerical simulations: Bulletin of Volcanology, v. 68, p. 462–479.

Valade, S., Lacanna, G., Coppola, D., Laiolo, M., Pistolesi, M., Donne, D.D., Genco, R., Marchetti, E., Ulivieri, G., Allocca, C., Cigolini, C., Nishimura, T., Poggi, P., and Ripepe, M., 2016, Tracking dynamics of magma migration in open-conduit systems: Bulletin of Volcanology, p. 1–12, doi: 10.1007/s00445-016-1072-x.

Walter, T.R., Haghighi, M.H., Schneider, F.M., Coppola, D., Motagh, M., Saul, J., Babeyko, A., Dahm, T., Troll, V.R., Tilmann, F, Heimann, S., Valade, S., Triyono, R., Khomarudin, R., Kartadinata, N., Laiolo, M., Massimetti, F., Gaebler, P., 2019, Complex hazard cascade culminating in the Anak Krakatau sector collapse: Nature Communications, doi: 10.1038/s41467-019-12284-5

Ward, S.N., and Day, S., 2003, Ritter Island volcano–Lateral collapse and the tsunami of 1888: Geophysical Journal International, v. 154, p. 891–902.

Wyering, L.D., Villeneuve, M.C., Wallis, I.C., Siratovich, P.A., Kennedy, B.M., Gravley, D.M., Cant, J.L., 2014, Mechanical and physical properties of hydrothermally altered rocks, Taupo Volcanic Zone, New Zealand: J. Volcanol. Geotherm. Res., v. 288, p. 76-93.

FIGURE CAPTIONS

Figure 1. (A) Location of the three trenches. a-a’ topographic profile of Fig. 2 is shown (yellow dots: topographic control points; red dots: elevation of trench corners; green dots: elevation of the different layers in the trenches). (B) Tsunami and tephra sequences in the trenches. Length of

314 layers reflects differences in grain-size according to the scale above. Image in (A) is from
315 TerraMetrics, ©2018 Google.
316
317 Figure 2. (A) Topographic profile (red line) for a segment cross-cutting the trench area (Fig. 1)
318 obtained from a 1×1 m-spaced raster dataset combined with control points (yellow dots) and
319 theodolite measurements. (B) Thickness variation for LTD. (C) Mdϕ trend (straight line, left
320 axis) and average pebble volume trend at each site (dashed line, right axis) for LTd.
321
322 Figure 3. (A) Md_ϕ vs σ_ϕ plot of representative samples collected from the three tsunamis
323 (different symbols) at different trenches (different colors). Decreasing marker size indicates
324 increasing distance from the shore. The yellow star refers to a representative matrix sample of
325 beach sand. (B) Equivalent volumes of LTd pebbles at varying distance from the coast. (C)
326 Equivalent volume variability in pebbles from the three tsunami deposits.
327
328 Figure 4. Back-scattered images showing (A) the variability of components in deposit T2a
329 (juvenile scoriae and crystal fragments, holocrystalline clasts, and scoriae with leached rims); (B)
330 clast in T2a with mm-thick rim of leached glass; (C) juvenile, vesicular LP pumice clast from
331 T2a; (D) scoriaceous, HP juvenile clast from T2a. Scale bars are 100 μm. (E) SiO_2 vs K_2O plot
332 showing the chemical variability of matrix glass in the different tephra layers. The dashed lines
333 indicate the variability of high-porphyritic (HP) and low-porphyritic (LP) magmas.
334
335 [1]GSA Data Repository item 201Xxxx, including methods used for topographic, sedimentological
336 and chemical data acquisition, is available online at www.geosociety.org/pubs/ft20XX.htm, or

by request from editing@geosociety.org or Documents Secretary, GSA, P.O. Box 9140, Boulder, CO 80301, USA.

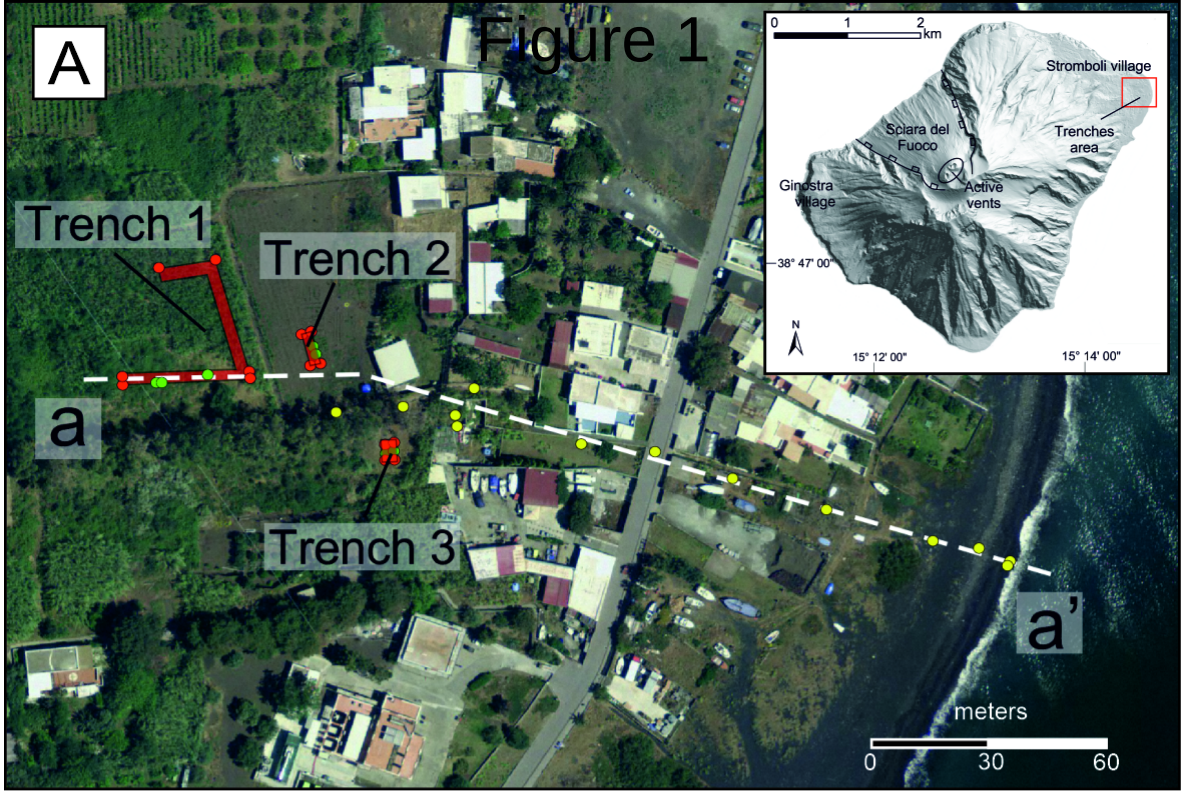
A
Figure 1
Trench 1
Trench 2
Trench 3
a
a'
meters
0
30
60
0
1
2
km
Stromboli village
Trenches area
Sciara del Fuoco
Ginostra village
Active vents
38° 47' 00"
15° 12' 00"
15° 14' 00"
N

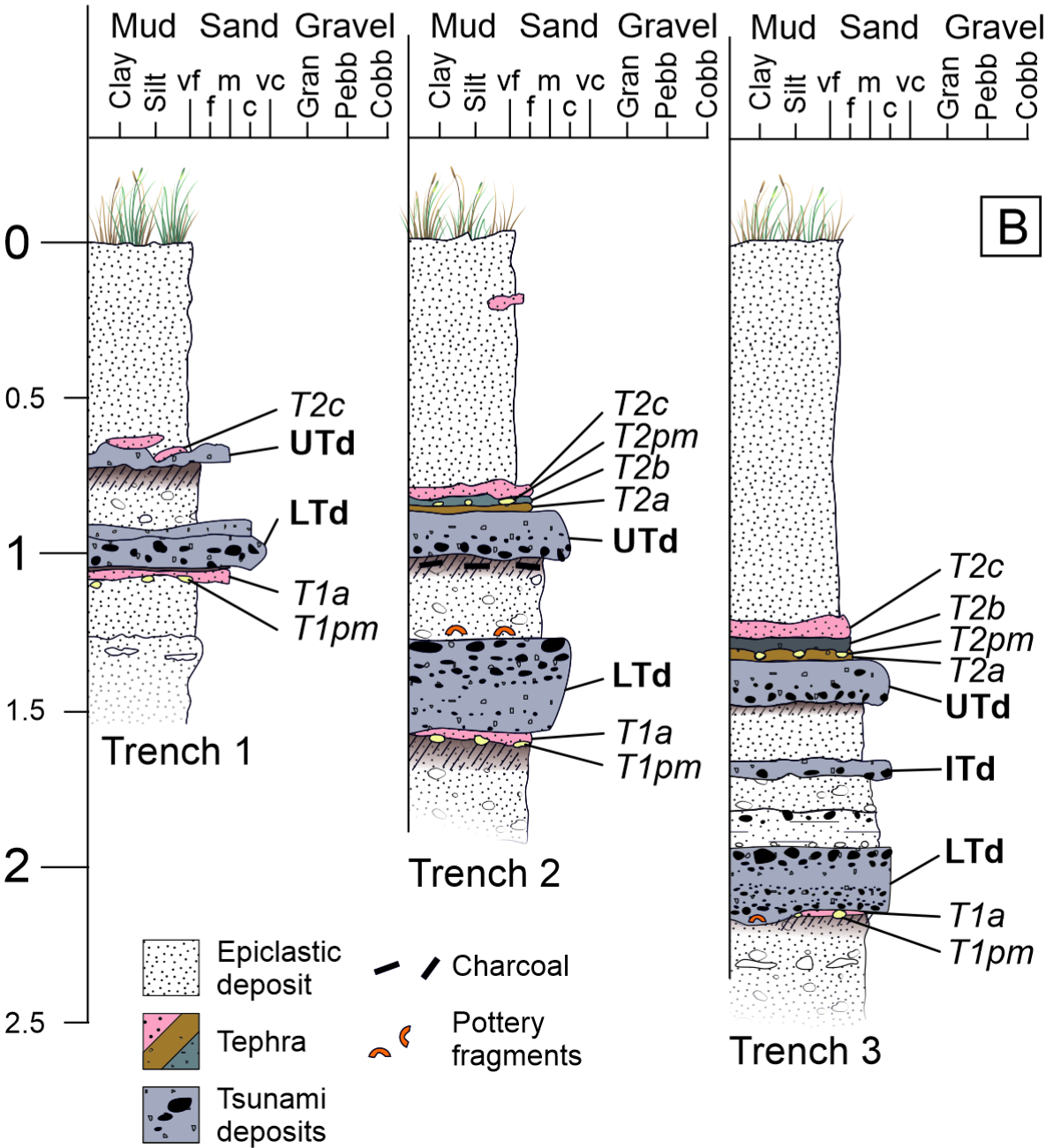
Mud
Sand
Gravel
Clay
Silt
vf
f
m
c
vc
Gran
Pebb
Cobb
0
0.5
1
1.5
2
2.5
T2c
UTd
LTd
T1a
T1pm
Trench 1
T2c
T2pm
T2b
T2a
UTd
LTd
T1a
T1pm
Trench 2
B
T2c
T2b
T2pm
T2a
UTd
ITd
LTd
T1a
T1pm
Trench 3
Epiclastic deposit
Tephra
Tsunami deposits
Charcoal
Pottery fragments

Figure 2

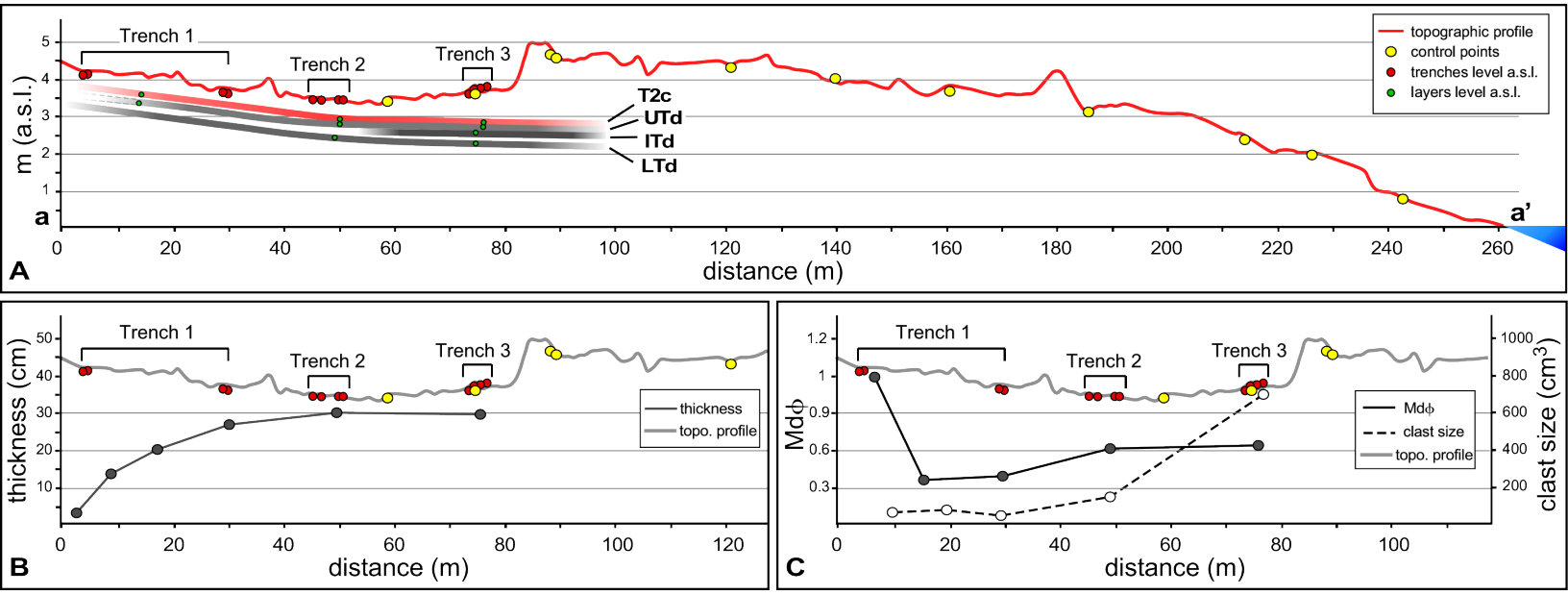
Trench 1
Trench 2
Trench 3
T2c
UTd
ITd
LTd
topographic profile
control points
trenches level a.s.l.
layers level a.s.l.
m (a.s.l.)
a
a'
distance (m)
A

Trench 1
Trench 2
Trench 3
thickness
topo. profile
thickness (cm)
distance (m)
B

Trench 1
Trench 2
Trench 3
Mdϕ
clast size
topo. profile
Mdϕ
clast size (cm³)
distance (m)
C

Figure 3

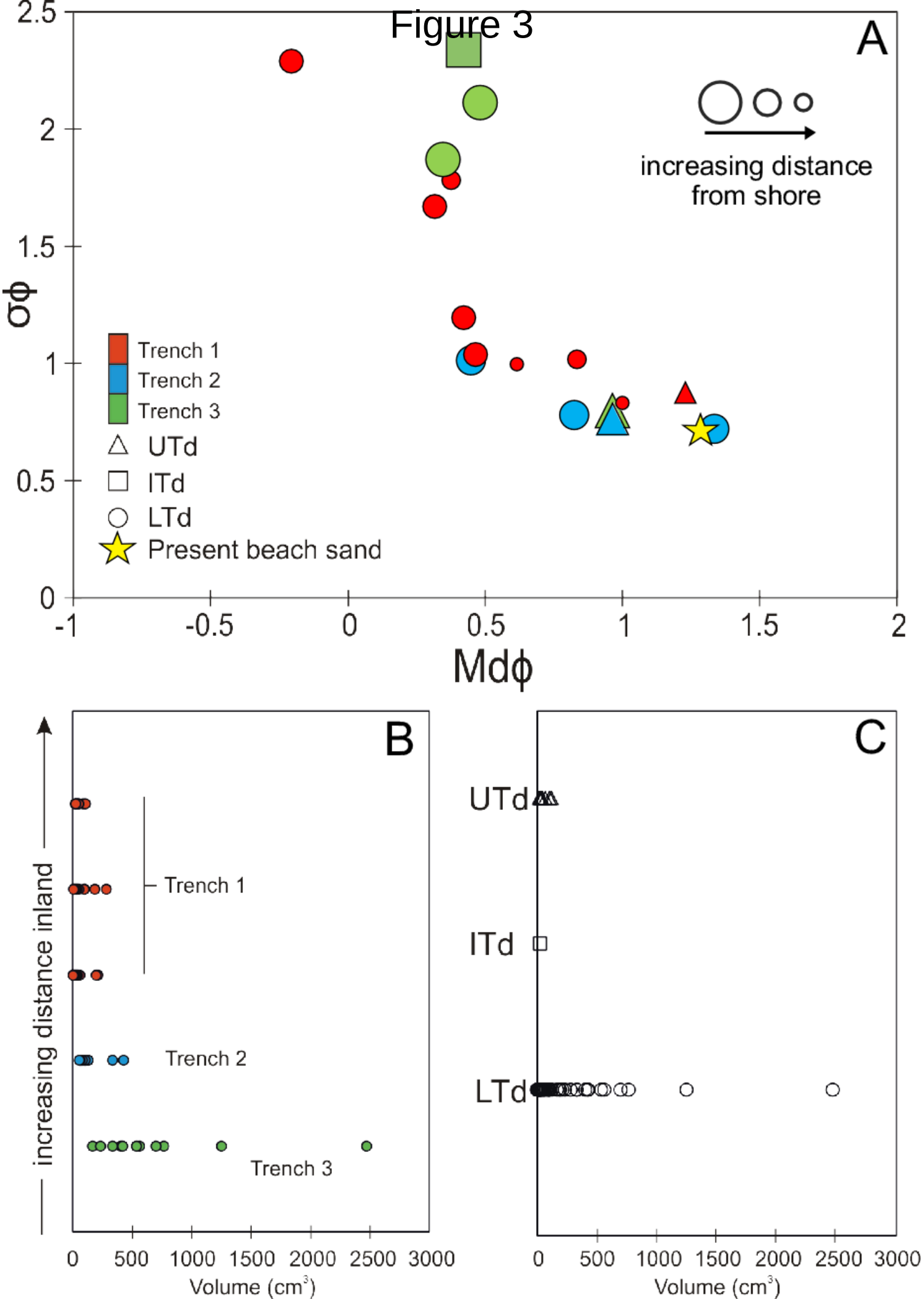
A
increasing distance
from shore
σϕ
Mdϕ
2.5
2
1.5
1
0.5
0
-1
-0.5
0
0.5
1
1.5
2
Trench 1
Trench 2
Trench 3
UTd
ITd
LTd
Present beach sand
B
increasing distance inland
Trench 1
Trench 2
Trench 3
0
500
1000
1500
2000
2500
3000
Volume (cm³)
C
UTd
ITd
LTd
0
500
1000
1500
2000
2500
3000
Volume (cm³)

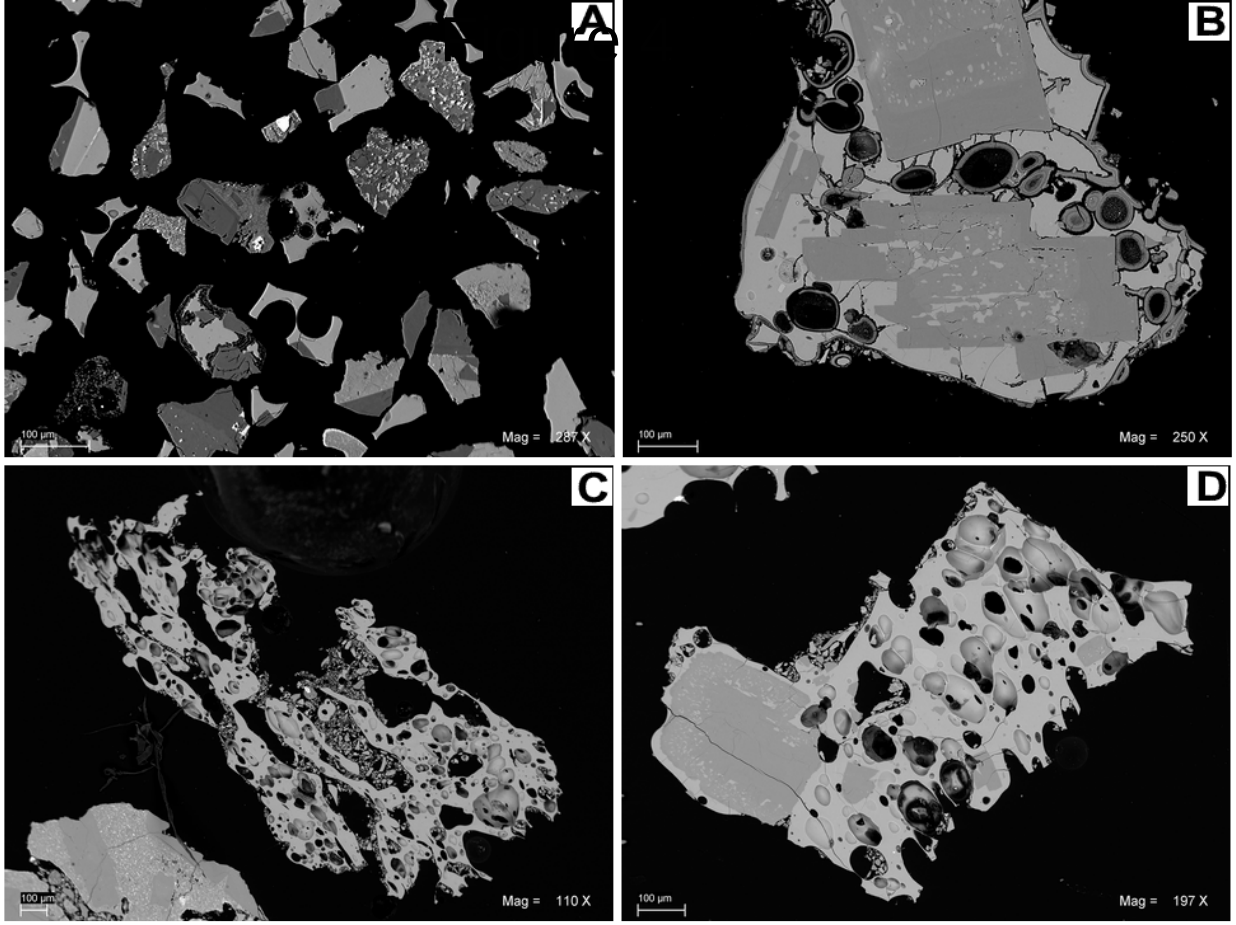
A
Mag = 287 X
100 µm
B
Mag = 250 X
100 µm
C
Mag = 110 X
100 µm
D
Mag = 197 X
100 µm

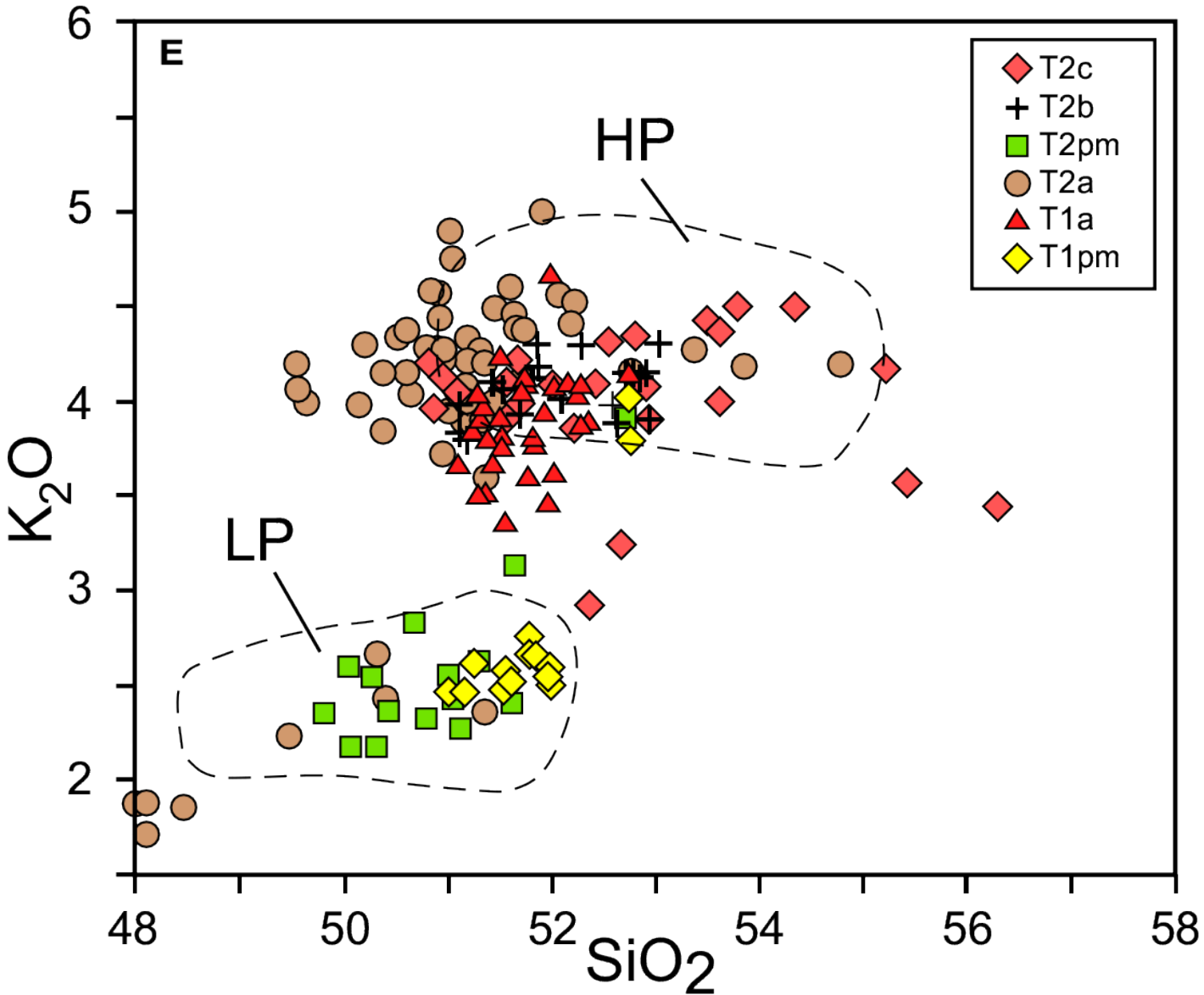
E
HP
LP
T2c
T2b
T2pm
T2a
T1a
T1pm
K2O
SiO2
6
5
4
3
2
48
50
52
54
56
58